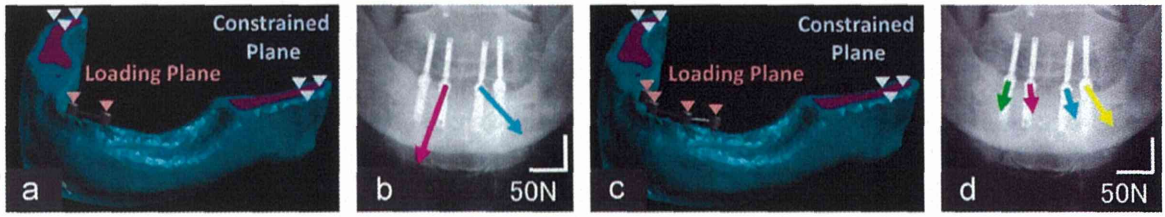

Fig. 2. Finite element models and measured load vectors in two test conditions. ((a) and (b)) 2 implants supported overdenture (2-OD), ((c) and (d)) 4 implants supported overdenture (4-OD). The arrows indicate load vector exerted on each implant in coronal plane. The model consists of cortical bone, cancellous bone, implants and bar attachments. The loads were applied on the upper plane of individual implants where the load measuring devices were mounted. The interface between implants and the surrounding bone were completely fixed and the part of mandibular ramus was completely constrained.

mandibular plane and sagittal plane. Measurements were conducted for two types of overdentures: 4 implants supported overdenture (4-OD) and 2 implants (locating medially) supported overdenture (2-OD) (Fig. 1e and f). The overdenture had 3 clip attachments that were connected with bar splinting 4 implants during function for 4-OD, only a clip at the center was connected with a bar splinting 2 implants for 2-OD (Fig. 1g). In 2-OD case, the distal implants (Imp1 and Imp4) were not contacted to the inner surface of denture during function. Clenching task was repeated five times for each condition. To avoid the influence of fatigue, duration of each clenching was 2 s with the interval of 2 min. Check bites were taken with silicone impression material (FLEXICON, GC Corporation, Tokyo, Japan) to make sure that the occlusal contact pattern was identical in both cases of 4-OD and 2-OD.

This study was approved by the research ethics committee of Tohoku University Graduate School of Dentistry.

4-OD and 2-OD FEA models were constructed with an ensemble of computer-aided-engineering software (Fig. 2).

(1) The CT data was converted to the JPEG images for shape extraction. Model geometry of the mandible was constructed from the images of the subject with dedicated software (Mechanical Finder, Research Center Of Computational Mechanics Inc, Tokyo, Japan). The region of mandible comprising cortical bone layer around a cancellous bone core was obtained by setting a threshold for the image data.
(2) The geometry of the implants (3.75 mm in diameter/13 mm in length) and the bar attachment were constructed with CAD software (Solidworks, Solidworks Corp, Concord, MA, USA).
(3) The position and angulation of each implant were determined with reference to X-ray cephalometric images of the subject (Fig. 3 and Table 1) and each implant was implemented into the model with FEA software (Patran, MSC Software, Santa Ana, CA, USA).

The interface between the implants and the surrounding bone was completely fixed to simulate the state of osseointegration. The part of mandibular ramus was completely constrained by enforcing zero-displacement conditions for all nodes (Fig. 2). All materials were assumed to be linear elastic isotropic behavior and material volumes were considered as homogeneous (Table 2) [25,26]. The model consisted of 126,134 ten-node tetrahedral elements and 196,198 nodes for 4-OD model and 135,420 elements and 180,830 nodes for 2-OD model.

The loads were applied on the upper plane of individual implants where the load measuring devices were mounted. Magnitude and direction of loads applied on the individual implants were the mean values of the loads on the respective implants, measured in the subject during her maximal voluntary clenching (MVC) (the arrows in Fig. 2b and d and Table 3).

The linear static stress analysis of those two models was conducted by FEA solver program, MSC Marc (MSC Software, LA, CA, USA) with TX7/i9610 supercomputer (Cyberscience Center, Tohoku University, Japan). The von Mises stress, the minimum principal stress, and the maximum principal stress were used to observe stress distribution. In the present study, we introduced the stresses contour maps for qualitative evaluation of the stress distributions comparatively between 2-OD and 4-OD. On the other hand, we introduced the two scalar-valued evaluation factors, σ_R and V_R for quantitative evaluation of the stress values defined as follows [21]:

σ_R: Average von Mises stress in 5 mm^3 stress concentration area around peri-implant bone (MPa). Before identifying the σ_R, von Mises stress of each element around each implant was calculated, and the elements were realigned in higher stress sequence up to 50 mm^3 in sum of the element volume for the implant. Then σ_R was calculated as the average of the stress in these elements.

V_R: Volume of von Mises stress concentration area (mm^3) (criteria: more than 3 MPa for the von Mises stress).

These two scalar-valued evaluation factors were computed for the von Mises stress in a columnar-shaped domain of the bone surrounding each implant.

3. Results

Distributions of von Mises stress, the minimum and maximum principal stresses in cortical bone for both models (2-OD and 4-OD) are shown in Fig. 4. Distributions of von Mises stress, the minimum and maximum principal stresses are also displayed in two cross-sectional planes: the first plane included the center points of the upper plane of Imp2 and Imp3 and perpendicular to *X–Y* plane, *i.e.* mandibular plane, and the second plane included the center points of the upper plane of Imp1 and Imp4 as shown in Figs. 5–7. Associated scalar-valued evaluation factors, σ_R and V_R are shown in Table 4. Here 3 MPa was used to define V_R because the value of σ_R for the implants in 4-OD, showing smallest σ_R, was approximately equal to 3 MPa. For this reason, we defined the area where von Mises stress exceeds 3 MPa as stress concentration area namely V_R for this analysis.

3.1. 2 Implants supported model (2-OD model)

In cortical bone, higher von Mises stress was observed around the neck of each implant (Fig. 4a and Fig. 5a). The minimum and maximum principal stress were higher in the distal and mesial side of each implant, respectively (Fig. 4a). In cancellous bone, relatively lower stresses were observed at implant thread parts (Fig. 4a, Fig. 6a and Fig. 7a)

The stress concentration factor σ_R was 4.90 MPa and the volume of stress concentration V_R was 78.0 mm^3 in Imp2, and 6.01 MPa and 64.0 mm^3 in Imp3, respectively (Table 4).

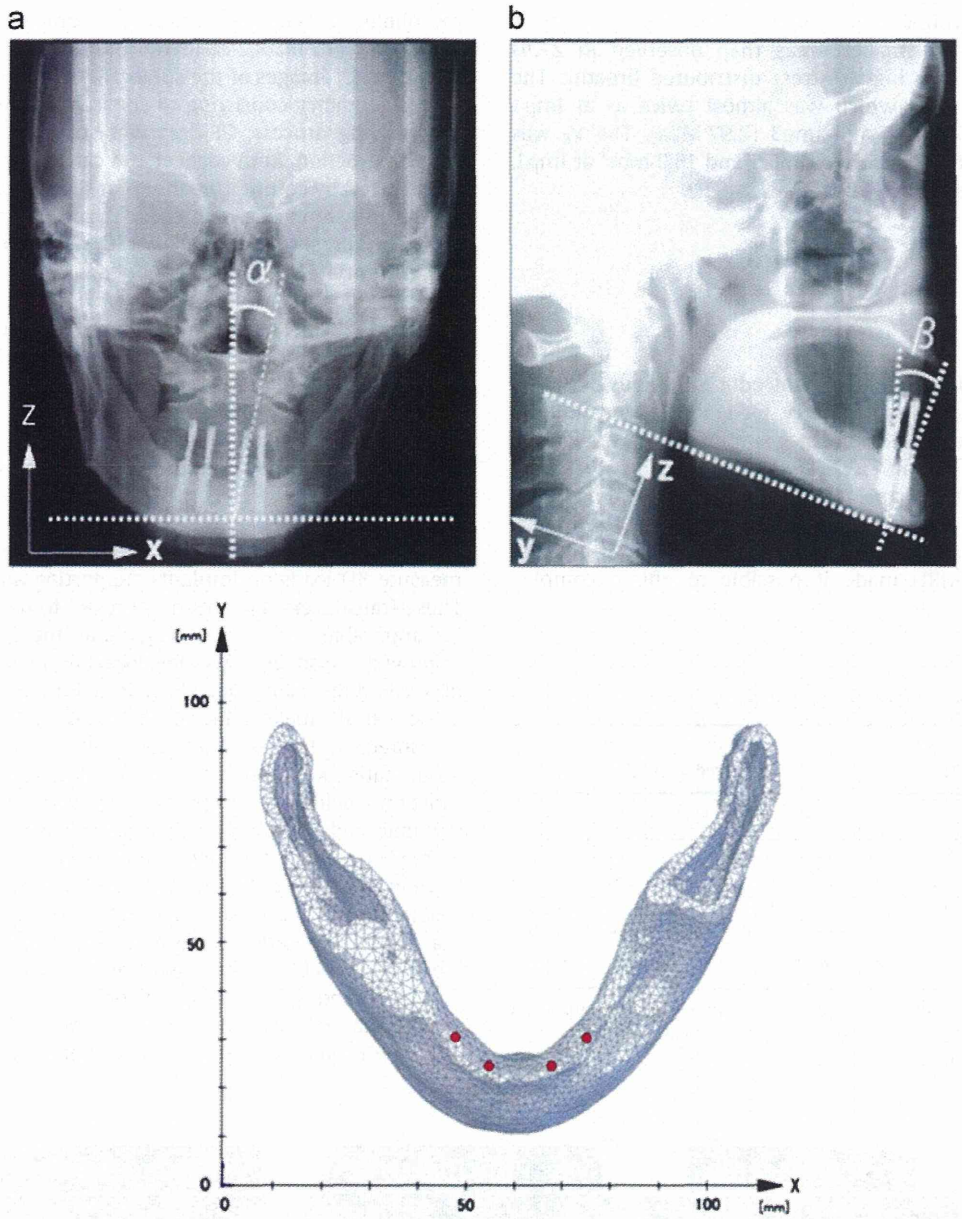

Fig. 3. Definition of the insertion positions and angulations of each implant. The position and angulation were determined with reference to X-ray cephalometric analysis. (a) The angulation of each implant in x–z plane defined as α (degree), (b) the angulation of each implant in y–z plane as β (degree) (c) the position of each implant was also defined with cephalometric analysis and implemented in the models.

Table 1
The insertion positions and angulations of each implant.

	X (mm)	Y (mm)	Z (mm)	α°	β°
Imp1	48.3	30.8	28.9	11.0	−12.5
Imp2	55.2	24.8	28.5	7.0	−15.5
Imp3	68.2	24.8	28	6.5	−17.5
Imp4	75.2	30.8	25.9	1.0	−25.0

The positions and angulations of each implant were determined with reference to X-ray cephalometric analysis.

Table 2
Material properties.

	Young's modulus (MPa)	Poisson's ratio
Implant (Ti)	106,330	0.34
Cortical bone	14,400	0.34
Cancellous bone	480	0.23

All materials were assumed to be linear elastic isotropic behavior and material volumes were considered as homogeneous. Young's modulus and Poisson's ratio were determined from literature.

3.2. 4 Implants supported model (4-OD model)

Similar to 2-OD model, stress concentration was observed for 4-OD model in cortical bone around each implant and low stresses were observed at implant thread part in cancellous bone (Figs. 4–7). On the other hand, the stress distributions were dependent on the definition of stresses and were quite irregular.

The minimum principal stress was higher in the distal side of Imp1, Imp3 and Imp4, and in the mesial side of Imp2 (Figs. 4 and 6b). The maximum principal stress was higher in the mesial side of Imp1, Imp3 and Imp4, and in the distal side of Imp3 (Figs. 4 and

7b). To summarize, around Imp1, Imp2 and Imp3, higher stress distributed in relatively smaller areas than observed in 2-OD model, but around Imp4, higher stress distributed broadly. The σ_R at Imp4 was 4.82 MPa which was almost twice as at Imp1 (2.66 MPa), Imp2 (2.70 MPa) and Imp3 (2.97 MPa). The V_R was 66.0 mm^3 at Imp4, whereas it was 4.8, 6.5 and 16.0 mm^3 at Imp1, Imp2 and Imp3, respectively (Table 4).

4. Discussion

4.1. FEA modeling

Previous FEA studies in dentistry introduced various simplifying assumptions in modeling geometry, load, boundary condition, and material properties, and so on. Such simplifications are known to affect the analytical result [16,27].

In the living body, the shape, quality, and quantity of bone have individual variability, which significantly influences the prognosis of implant treatment. Recent development of digital imaging techniques (CT and MRI) made it possible to obtain complex morphological data and improved accuracy of geometrical modeling of FEA [16,18,28,29]. In the present study, a series of image data from CT images of the subject was binarized to construct FEA model geometry consisting of cortical bone and cancellous bone. In modeling process, CT data was converted to JPEG format for shape extraction. Both cortical and cancellous bone geometry was constructed by setting threshold for JPEG data with 256 Gy levels. As the transition between cortical and cancellous bone was not clear, the threshold was decided by setting in a stepwise manner for appropriate geometrical modeling. Thus thickness of cortical bone has local variability.

Occlusal load exerted on implants varies depending upon forces generated by multiple masticatory muscles. Muscles activities, as well as craniofacial morphology, influence the magnitude and direction of the occlusal load [30–32]. Although a few previous FEA studies have simulated muscle forces in various manners [18,33,34], it is currently difficult to duplicate individual muscle activity to FEA modeling. Thus it is customary to use vertical or oblique load on teeth or implants as input load in FEA [17,26].

Meriske-Stern et al. [35] used piezoelectric transducers to measure 3D loads on implants supporting an overdenture *in vivo*. These transducers have been improved to be much smaller and to be applicable to *in vivo* sequential measurements. Using the improved transducers, we developed an *in vivo* measuring system of three-dimensional loads exerted on implants [21,22]. In the present study, mean values of the loads on the respective implants, measured in the subject during her MVC, were used as the input static load. Hence, the exerted loads on the implants during function including mastication of various foods show much dynamic and complicated manner, it is obvious that the loading scenario used in the present study is only a fragment of functional loading condition of the implants and do not completely describe a whole loading condition. It had better be taken into account for a real loading condition in future. Bonnet et al. conducted an FEA study of mandible bone supporting a four-implant retained bridge and examined the influence of foodstuff position [36]. They suggested that critical compressive stress induced in the case of foodstuff on molar position. The authors have measured the loads

Table 3
Measured load values during MVC in two test conditions.

	2-OD Measured value (N)					4-OD Measured value (N)			
	$f(x)$	$f(y)$	$f(z)$	$\|f\|$		$f(x)$	$f(y)$	$f(z)$	$\|f\|$
Imp1	–	–	–	–	Imp1	−11.4	10.7	−41.1	44.0
Imp2	−38.0	6.2	−106.0	112.8	Imp2	3.2	−11.0	−39.8	41.5
Imp3	55.8	0.3	−63.4	84.4	Imp3	11.1	−12.1	−40.3	43.5
Imp4	–	–	–	–	Imp4	33.2	0.1	−54.5	63.8
Total				197.2	**Total**				192.8

The magnitude and direction of the loads applied on the individual implants of FEA were mean values of the loads on the respective implants, measured in the subject during her maximal voluntary clenching.

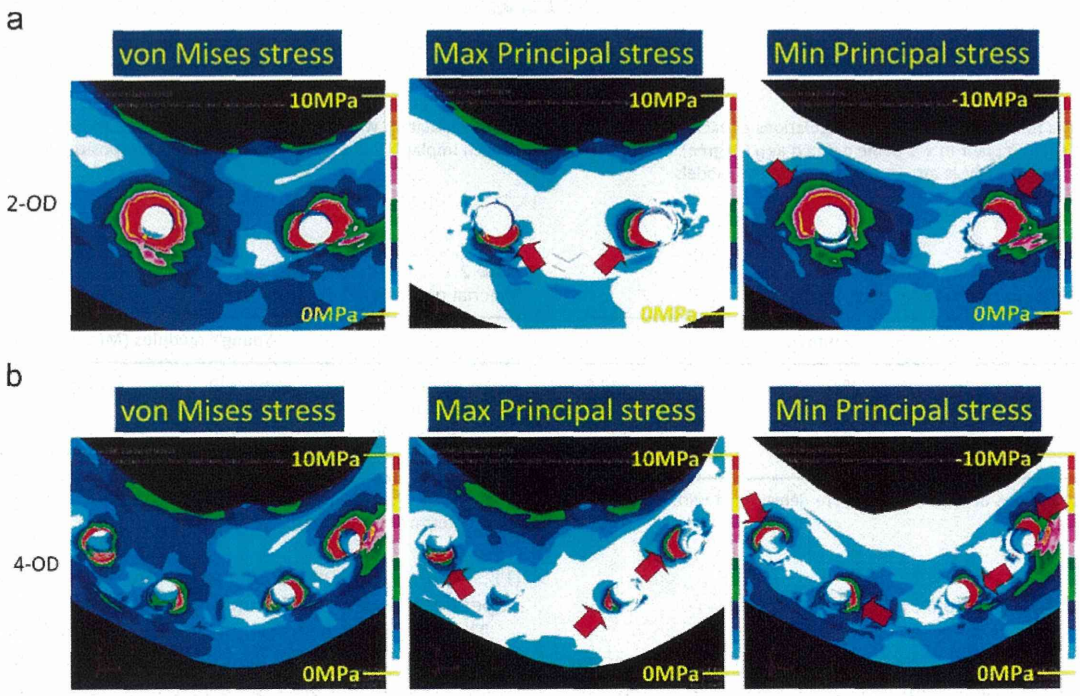

Fig. 4. Stress distribution shown on the out surface of the model. (a) 2 Implants supported overdenture (2-OD), (b) 4 implants supported overdenture (4-OD).

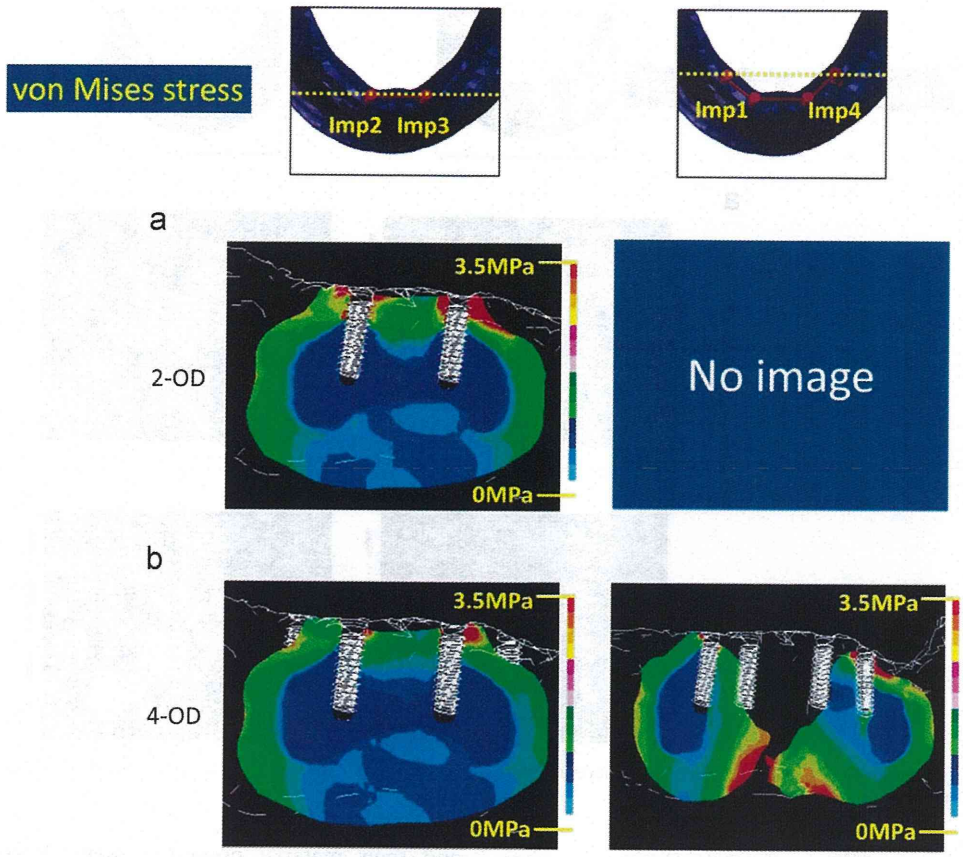

Fig. 5. Cross sectional view of von Mises stress distribution in cortical and cancellous bone. (a) 2 Implants supported overdenture (2-OD), (b) 4 implants supported overdenture (4-OD).

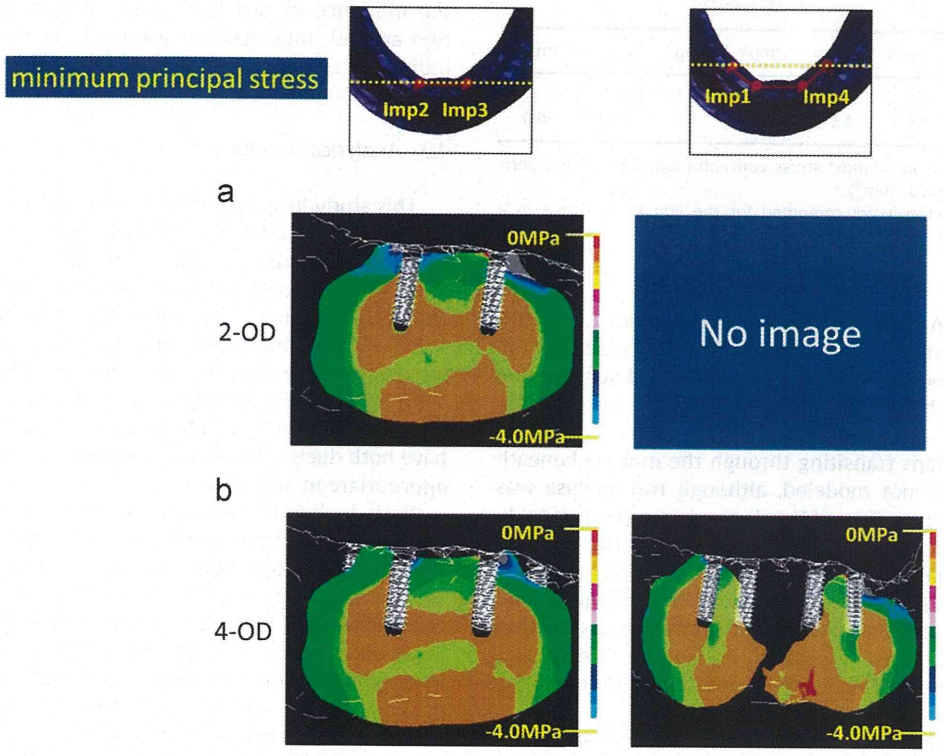

Fig. 6. Cross sectional view of the minimum principal stress distribution in cortical and cancellous bone. (a) 2 Implants supported overdenture (2-OD), (b) 4 implants supported overdenture (4-OD).

on the implants during chewing of various foods and during biting wax on the either side of the denture in the same subject. The measured load vector varied dynamically time by time in terms of its direction and magnitude, and the norms of the vectors were relatively smaller than those during her MVC. The results of trial analyses using these functional loads as the input loading data

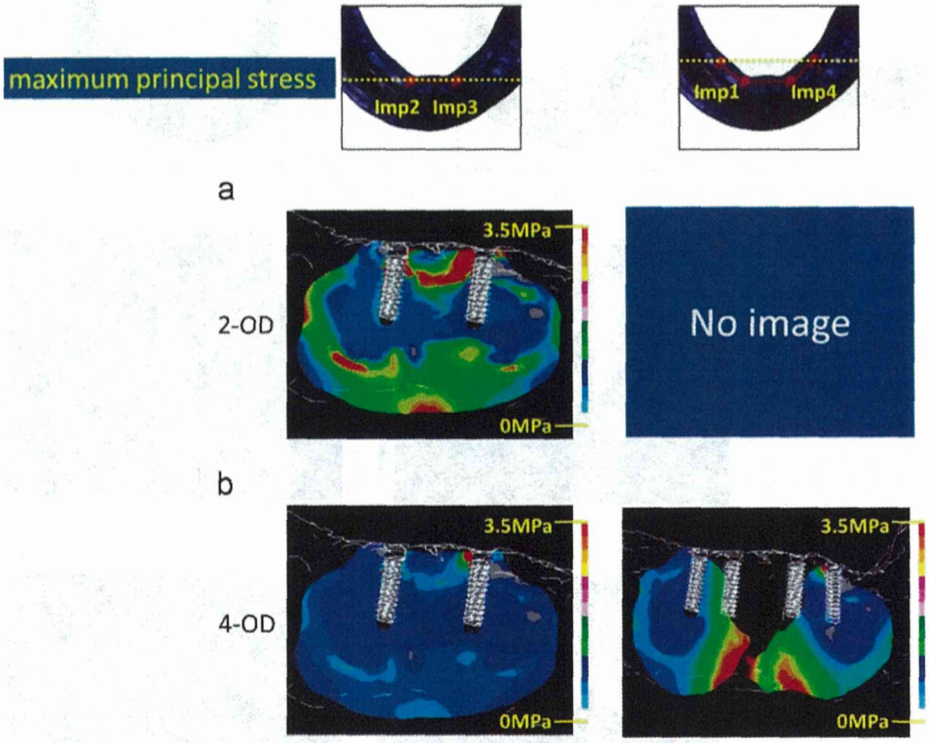

Fig. 7. Cross sectional view of the maximum principal stress distribution in cortical and cancellous bone. (a) 2 Implants supported overdenture (2-OD), (b) 4 implants supported overdenture (4-OD).

Table 4
Scalar-valued evaluation factors computed for the von Mises stress (σ_R and V_R).

	σ_R (MPa)				V_R (mm^3)			
	Imp1	Imp2	Imp3	Imp4	Imp1	Imp2	Imp3	Imp4
2-OD	–	4.9	6.0	–	–	78.0	64.0	–
4-OD	2.7	2.7	3.0	4.8	4.8	6.5	16.0	66.0

σ_R: Average von Mises stress in 50 mm^3 stress concentration area around peri-implant bone (MPa).V_R: Voluma (mm^3).
Scalar-valued evaluation factors were computed for the von Mises stress in a columnar-shaped domain of the bone surrounding each implant.

to the same static FEA model employed in this study were rather difficult to comprehend the stress distribution caused by the difference of the number of supporting implants and surrounding bone structure. Thus, the authors decided to use the loads during her MVC for analyses.

In this study, the loads transiting through the mucosa beneath the denture base were not modeled, although the mucosa was contacted with the inner surface of her denture in molar region. In both case of 4-OD and 2-OD, total occlusal force on the denture, total loads on the implants were not significantly different and the contact area beneath the denture to mucosa were identical and away from Imp1 and Imp4, so that the influence was assumed to be relatively small. For further detailed analysis, it is definitely important to reproduce realistic loading conditions and to employ dynamic analyzing method.

In this study, biological data such as CT data and measured load from a certain subject was successfully duplicated to the FEA models. The cortical bone and cancellous bone are both heterogeneous and have anisotropic mechanical properties [37]. It has been reported that bone anisotropy significantly affects stresses and strains in peri-implant bone [26]. Yet, in the present study, cortical bone and cancellous bone were assumed to be isotropic and their material properties were determined according to literatures for simplicity. This simplification would be permissible, because main objective of the present paper was to investigate the influence of real load in her mouth on the stress distribution around implants. It is a topic in future research to consider individual anisotropic material properties (transversely isotropic) and inhomogeneities of bone.

4.2. Analytical results

This study focused on the mechanical stress in the peri-implant bone. In FEA studies to evaluate mechanical stress in the peri-implant bone, it is customary to use stresses of various kinds, such as von Mises stress, the maximum, the minimum principal stress and the maximum shear stress. The maximum principal stress is suited for the observation of tensile stress and the minimum one for compressive one, whereas the von Mises stress is the most commonly and primarily used scalar-valued stress invariant to evaluate yielding/failure behavior of various materials. Since bone have both ductile and brittle response, the use of principle stress is appropriate in such studies.

Both in 2-OD model and 4-OD model, distributions of such stresses in peri-implant bone were complex due to *in vivo* loads (Fig. 4). As a whole, high stress mainly distributed in cortical bone around implants, whereas low stress distributed in cancellous bone, regardless the definition of stress (Figs. 5–7). Such low stress in cancellous bone might be ascribed to the binarization of material properties. Although cancellous bone showed low stress distributions, it doesn't contradict the risk of bone damage or modeling. It has been reported lower stress affect the activation of bone metabolism in cancellous bone [14].

In 2-OD model, cortical bone around each implant showed high stress distribution in different directions: the mesiodistal direction for the von Mises stress, the mesial direction for the maximum principal stress, and the distal direction for the minimum principal stress (Fig. 4a). These tendencies might reflect the *in vivo* load

direction of each implant (Fig. 2b). Imp3 had higher stress concentration and Imp2 had a larger volume of stress concentration (Table 4). Such lack of bilateral symmetry might be ascribed to the characteristic of this particular subject, *i.e.* inclination of each implant, loading conditions and peri-implant bone conditions, which cannot be accounted for without having biological data.

In 4-OD model, high stresses also distributed in various directions with the definition of stresses (Fig. 4b), which was affected by the *in vivo* load direction (Fig. 2d) similar to 2-OD model. In particular, higher and wider stress concentration was observed around Imp4 with a large inclination of load direction and with thin supporting cortical bone. Influence of cortical bone thickness on stress around implants has been reported in previous study [38]. The stress concentration observed around Imp4 also shows the importance of biological-data-based FEA.

In the present study, we introduced the two scalar-valued evaluation factors (σ_R and V_R) to evaluate the stress concentration area comparatively between 2-OD and 4-OD. This evaluation method was effective to grasp the spatial distribution of mechanical stress in an averaged sense. Within the limitations of this analysis, we defined criteria of these values. Therefore, the criteria of scalar-valued evaluation factors might needs to examine in each analysis.

The total amount of load applied to the implant was 197.2 (N) in 2-OD model and was almost identical with that of 192.8 (N) in 4-OD model (Table 3). In 4-OD model, all implants, except for Imp4, displayed obviously lower evaluation factors than 2-OD model (Table 4). Stress reduction in 4-OD model might be related to the higher rigidity of 4-OD model being connected with the bar attachment. A similar effect of splinting implants with bar attachment in a mandibular overdenture was reported in previous study [39]. Furthermore, stress reduction by increasing the number of implants was also reported by *in vitro* experimental studies [40,41]. Silva et al. reported comparative FEA study of prostheses supported by four or six implants [42]. They concluded increasing the number of implants induced reduction of von Mises stress values and the cantilever greatly increase stress on the distal implant. These results are in common with the present results. Although the biological data were obtained from only one subject, the present result suggests 4-OD model can reduced the overloads compared with 2-OD model, which differs from the conclusion of Meijer et al. They concluded that there is no reduction of the extreme principal stresses by increasing the number of implants on two *versus* four implants in edentulous mandible FEA [43]. Such inconsistency might be caused by the different evaluation methods of spatial stress distribution in an averaged sense (σ_R and V_R) and implementation of *in vivo* load data in FEA.

Regardless of the stress reduction achieved in 4-OD model, higher stress distributed around Imp4. This might be owing to a large deviation of load direction from the alignment of Imp4 and also to thin supporting cortical bone. The difference between load direction and implant alignment was larger in the mesiodistal direction than in the buccolingual direction, and, accordingly high stress distributed in the mesiodistal direction around Imp4. This indicates the stress distribution around an implant strongly depends on *in vivo* load direction, and also shows the importance of the implementation of individual variability into FEA analysis. Interaction of load direction on stress distribution has been reported in previous study [44,45]. The rigidity and deflection of prosthetic materials and stress concentration (overloads) contribute to clinical complications, such as screw loosening and fracturing of the prosthetic component [4,16]. Hence, stress reduction achieved in 4-OD model would possibly make the risk of clinical complications lower. In addition, it is reported that mechanical stress plays an essential role in maintaining homeostasis of the bone [46] and occlusal overload could be one of the risk factor for peri-implant bone loss in animal model [9]. Demenko et al. conducted an FEA study, suggesting to choose implant size with due consideration of its load-carrying capacity [47]. Barbier et al. reported a comparative study of FEA and animal experiment and concluded that the highest bone remodeling events coincided with high equivalent stress area and that major remodeling difference between axial and non-axial load was mainly ascribed to the horizontal component of stress [48]. In long-term results of mandibular implants supported overdenture, it has been reported that loss of osseointegration without signs of infection was more frequent than peri-implantitis [5]. These associations indicate the importance of biomechanical condition on implant-bone interfaces for long-term implant success. In this paper, we made clear that the number of implants and the individual bone geometry of the subject affected mechanical stress in the mandibular bone around implants. It indicates the possibility of biomechanical optimization of implant treatment based on biological data of a subject, possibly supported by an FEA analysis. Furthermore, it may contribute to decision of treatment design of implant treatment.

5. Conclusion

In the present study, we successfully constructed a biological-data-based FEA system from *in vivo* loads and CT data of a subject. Stress distribution was affected by magnitude and direction of the load and bone geometry. High von Mises stress was observed in cortical bone around implant neck. The stress around the supporting bone in 2 implants model was higher than that in 4 implants model to demonstrate the mechanical prominence of using more implants. Even in 4 implants model, high stress was found around an implant with a large inclination and with thin cortical bone. This suffices to demonstrate the capability and usefulness of the biological-data-based FEA.

Acknowledgments

This research was supported by a Grant-in-Aid for Scientific Research (No's 26462910) from the Japan Society for the Promotion of Science.

References

[1] H.P. Weber, C. Sukotjo, Does the type of implant prosthesis affect outcomes in the partially edentulous patient? Int. J. Oral Maxillofac. Implants 22 (Suppl.) (2007) 140–172.
[2] B. Koller, W. Att, J.R. Strub, Survival rates of teeth, implants, and double crown-retained removable dental prostheses: a systematic literature review, Int. J. Prosthod. 24 (2011) 109–117.
[3] H. Suito, Y. Tomotake, M. Watanabe, D. Nagao, Y. Ishida, T. Ichikawa, Survival of immediate implant restoration: a retrospective study through 9-year-observation, J. Prosthod. Res. 55 (2011) 141–145.
[4] C. Karabuda, M. Yaltirik, M. Bayraktar, A clinical comparison of prosthetic complications of implant-supported overdentures with different attachment systems, Implant Dent. 17 (2008) 74–81.
[5] T. Ueda, U. Kremer, J. Katsoulis, R. Mericske-Stern, Long-term results of mandibular implants supporting an overdenture: implant survival, failures, and crestal bone level changes, Int. J. Oral Maxillofac. Implants 26 (2011) 365–372.
[6] D. Pavlin, J. Gluhak-Heinrich, Effect of mechanical loading on periodontal cells, Crit. Rev. Oral Biol. Med.: An Official Publication of the American Association of Oral Biologists 12 (2001) 414–424.
[7] E. De Smet, J. Duyck, J. Vander Sloten, R. Jacobs, I. Naert, Timing of loading – immediate, early, or delayed – in the outcome of implants in the edentulous mandible: a prospective clinical trial, Int. J. Oral Maxillofac. Implants 22 (2007) 580–594.
[8] F. Isidor, Loss of osseointegration caused by occlusal load of oral implants. A clinical and radiographic study in monkeys, Clin. Oral. Implants Res. 7 (1996) 143–152.
[9] J. Duyck, H.J. Ronold, H. Van Oosterwyck, I. Naert, J. Vander Sloten, J.E. Ellingsen, The influence of static and dynamic loading on marginal bone

reactions around osseointegrated implants: an animal experimental study, Clin. Oral. Implants Res. 12 (2001) 207–218.
[10] I. Herrmann, U. Lekholm, S. Holm, C. Kultje, Evaluation of patient and implant characteristics as potential prognostic factors for oral implant failures, Int. J. Oral Maxillofac. Implants 20 (2005) 220–230.
[11] S. Hansson, M. Werke, The implant thread as a retention element in cortical bone: the effect of thread size and thread profile: a finite element study, J. Biomech. 36 (2003) 1247–1258.
[12] D. Bozkaya, S. Muftu, A. Muftu, Evaluation of load transfer characteristics of five different implants in compact bone at different load levels by finite elements analysis, J. Prosthet. Dent. 92 (2004) 523–530.
[13] L. Baggi, I. Cappelloni, M. Di Girolamo, F. Maceri, G. Vairo, The influence of implant diameter and length on stress distribution of osseointegrated implants related to crestal bone geometry: a three-dimensional finite element analysis, J. Prosthet. Dent. 100 (2008) 422–431.
[14] L. Baggi, I. Cappelloni, F. Maceri, G. Vairo, Stress-based performance evaluation of osseointegrated dental implants by finite-element simulation, Simul. Modell. Pract. Theory 16 (2008) 971–987.
[15] G. Vairo, G. Sannino, Comparative evaluation of osseointegrated dental implants based on platform-switching concept: influence of diameter, length, thread shape, and in-bone positioning depth on stress-based performance, Comput. Math. Methods Med. 2013 (2013) 250929.
[16] J.P. Geng, K.B. Tan, G.R. Liu, Application of finite element analysis in implant dentistry: a review of the literature, J. Prosthet. Dent. 85 (2001) 585–598.
[17] S. Lu, T. Li, Y. Zhang, C. Lu, Y. Sun, J. Zhang, D. Xu, Biomechanical optimization of the diameter of distraction screw in distraction implant by three-dimensional finite element analysis, Comput. Biol. Med. 43 (2013) 1949–1954.
[18] M. Daas, G. Dubois, A.S. Bonnet, P. Lipinski, C. Rignon-Bret, A complete finite element model of a mandibular implant-retained overdenture with two implants: comparison between rigid and resilient attachment configurations, Med. Eng. Phys. 30 (2008) 218–225.
[19] R.S. Pessoa, L. Muraru, E.M. Junior, L.G. Vaz, J.V. Sloten, J. Duyck, S.V. Jaecques, Influence of implant connection type on the biomechanical environment of immediately placed implants—CT-based nonlinear, three-dimensional finite element analysis, Clin. Implant Dent. Relat. Res. 12 (2010) 219–234.
[20] T. Kawata, N. Yoda, T. Kawaguchi, T. Kuriyagawa, K. Sasaki, Behaviours of three-dimensional compressive and tensile forces exerted on a tooth during function, J. Oral Rehabil. 34 (2007) 259–266.
[21] R. Shigemitsu, T. Ogawa, T. Matsumoto, N. Yoda, Y. Gunji, Y. Yamakawa, K. Ikeda, K. Sasaki, Stress distribution in the peri-implant bone with splinted and non-splinted implants by *in vivo* loading data-based finite element analysis, Odontology. 101 (2), 2013, 222–226.
[22] N. Yoda, Y. Gunji, T. Ogawa, T. Kawata, K. Sasaki, *In vivo* load measurement for evaluating the splinting effects of implant-supported superstructures: a pilot study, Int. J. Prosthod. 26 (2013) 143–146.
[23] U.Z. Lekholm, G.A., Patient selection and preparation, in: PI Brånemark, GA Zarb, T Albrektsson (Eds.), Tissue-integrated Prostheses, Quintessance Publishing Co, Chicago, 1985, pp. 199–209.
[24] T. Kawaguchi, T. Kawata, T. Kuriyagawa, K. Sasaki, *In vivo* 3-dimensional measurement of the force exerted on a tooth during clenching, J. Biomech. 40 (2007) 244–251.
[25] P.C. Dechow, G.A. Nail, C.L. Schwartz-Dabney, R.B. Ashman, Elastic properties of human supraorbital and mandibular bone, Am. J. Phys. Anthropol. 90 (1993) 291–306.
[26] A.M. O'Mahony, J.L. Williams, P. Spencer, Anisotropic elasticity of cortical and cancellous bone in the posterior mandible increases peri-implant stress and strain under oblique loading, Clin. Oral. Implants Res. 9 (2000) 648–657.
[27] A.G. Hannam, Current computational modelling trends in craniomandibular biomechanics and their clinical implications, J. Oral Rehabil. 38 (2011) 217–234.
[28] Y. Shimizu, K. Usui, K. Araki, N. Kurosaki, H. Takanobu, A. Takanashi, Study of finite element modeling from CT images, Dent. Mater. J. 24 (2005) 447–455.
[29] N. Wakabayashi, T. Kondo, R. Yahagi, T. Suzuki, A patient-based model study of fixed splinting of premolars with reduced periodontal support, Int. J. Comput. Dent. 13 (2010) 317–330.
[30] O. Plesh, B. Bishop, W.D. McCall, Patterns of jaw muscle activity during voluntary chewing, J. Oral Rehabil. 23 (1996) 262–269.
[31] K. Sasaki, A.G. Hannam, W.W. Wood, Relationships between the size, position, and angulation of human jaw muscles and unilateral first molar bite force, J. Dent. Res. 68 (1989) 499–503.
[32] T. Ogawa, T. Kawata, A. Tsuboi, Y. Hattori, M. Watanabe, K. Sasaki, Functional properties and regional differences of human masseter motor units related to three-dimensional bite force, J. Oral Rehabil. 33 (2006) 729–740.
[33] T.W. Korioth, A.G. Hannam, Deformation of the human mandible during simulated tooth clenching, J. Dent. Res. 73 (1994) 56–66.
[34] L. Baggi, S. Pastore, M. Di Girolamo, G. Vairo, Implant-bone load transfer mechanisms in complete-arch prostheses supported by four implants: a three-dimensional finite element approach, J. Prosthet. Dent. 109 (2013) 9–21.
[35] R. Mericske-Stern, P. Assal, W. Buergin, Simultaneous force measurements in 3 dimensions on oral endosseous implants *in vitro* and *in vivo*. A methodological study, Clin. Oral. Implants Res. 7 (1996) 378–386.
[36] A.S. Bonnet, M. Postaire, P. Lipinski, Biomechanical study of mandible bone supporting a four-implant retained bridge: finite element analysis of the influence of bone anisotropy and foodstuff position, Med. Eng. Phys. 31 (2009) 806–815.
[37] A.M. O'Mahony, J.L. Williams, J.O. Katz, P. Spencer, Anisotropic elastic properties of cancellous bone from a human edentulous mandible, Clin. Oral. Implants Res. 11 (2000) 415–421.
[38] N. Okumura, R. Stegaroiu, E. Kitamura, K. Kurokawa, S. Nomura, Influence of maxillary cortical bone thickness, implant design and implant diameter on stress around implants: a three-dimensional finite element analysis, J. Prosthod. Res. 54 (2010) 133–142.
[39] L.F. Tabata, W.G. Assuncao, V.A. Barao, E.A. Gomes, J.A. Delben, E.A. de Sousa, E. P. Rocha, Comparison of single-standing or connected implants on stress distribution in bone of mandibular overdentures: a two-dimensional finite element analysis, J. Craniofac. Surg. 21 (2010) 696–702.
[40] T. Ogawa, S. Dhaliwal, I. Naert, A. Mine, M. Kronstrom, K. Sasaki, J. Duyck, Impact of implant number, distribution and prosthesis material on loading on implants supporting fixed prostheses, J. Oral Rehabil. 37 (2010) 525–531.
[41] T. Ogawa, S. Dhaliwal, I. Naert, A. Mine, M. Kronstrom, K. Sasaki, J. Duyck, Effect of tilted and short distal implants on axial forces and bending moments in implants supporting fixed dental prostheses: an *in vitro* study, Int. J. Prosthod. 23 (2010) 566–573.
[42] G.C. Silva, J.A. Mendonca, L.R. Lopes, J. Landre Jr., Stress patterns on implants in prostheses supported by four or six implants: a three-dimensional finite element analysis, Int. J. Oral Maxillofac. Implants 25 (2010) 239–246.
[43] H.J. Meijer, F.J. Starmans, W.H. Steen, F. Bosman, A three-dimensional finite element study on two *versus* four implants in an edentulous mandible, Int. J. Prosthod. 7 (1994) 271–279.
[44] L. Qian, M. Todo, Y. Matsushita, K. Koyano, Effects of implant diameter, insertion depth, and loading angle on stress/strain fields in implant/jawbone systems: finite element analysis, Int. J. Oral Maxillofac. Implants 24 (2009) 877–886.
[45] T. Takahashi, I. Shimamura, K. Sakurai, Influence of number and inclination angle of implants on stress distribution in mandibular cortical bone with All-on-4 Concept, J. Prosthod. Res. 54 (2010) 179–184.
[46] A.G. Robling, A.B. Castillo, C.H. Turner, Biomechanical and molecular regulation of bone remodeling, Annu. Rev. Biomed. Eng. 8 (2006) 455–498.
[47] V. Demenko, I. Linetskiy, K. Nesvit, A. Shevchenko, Ultimate masticatory force as a criterion in implant selection, J. Dent. Res. 90 (2011) 1211–1215.
[48] L. Barbier, J. Vander Sloten, G. Krzesinski, E. Schepers, G. Van der Perre, Finite element analysis of non-axial *versus* axial loading of oral implants in the mandible of the dog, J. Oral Rehabil. 25 (1998) 847–858.

ADVANCED HEALTHCARE MATERIALS
www.advhealthmat.de

Characterization of the Attachment Mechanisms of Tissue-Derived Cell Lines to Blood-Compatible Polymers

*Takashi Hoshiba, Mayo Nikaido, and Masaru Tanaka**

Recent advances in biomedical engineering require the development of new types of blood-compatible polymers that also allow non-blood cell attachment for the isolation of stem cells and circulating tumor cells (CTCs) from blood and for the development of artificial organs for use under blood-contact conditions. Poly(2-methoxyethyl acrylate) (PMEA) and poly(tetrafurfuryl acrylate) (PTHFA) were previously identified as blood-compatible polymers. Here, it is demonstrated that cancer cells can attach to the PMEA and PTHFA substrates, and the differences in the attachment mechanisms to the PMEA and PTHFA substrates between cancer cells and platelets are investigated. It is also found that the adsorption-induced deformation of fibrinogen, which is required for the attachment and activation of platelets, does not occur on the PMEA and PTHFA substrates. In contrast, fibronectin is deformed on the PMEA and PTHFA substrates. Therefore, it is concluded that cancer cells and not platelets can attach to the PMEA and PTHFA substrates based on this protein-deformation difference between these substrates. Moreover, it is observed that cancer cells attach to the PMEA substrate via both integrin-dependent and -independent mechanisms and attach to the PTHFA substrate only through an integrin-dependent mechanism. It is expected that PMEA and PTHFA will prove useful for blood-contact biomedical applications.

1. Introduction

The regulation of cell attachment through the use of biomaterials is an important issue in biomedical applications, such as cell patterning for drug testing cell arrays, the reconstruction of vascular and neural systems in vitro, and specific cell isolation.[1–4] In particular, blood-compatible materials that prevent blood cell attachment have been extensively studied because these materials can be used for blood-contact biomedical applications.[5–7] Several materials that are capable of suppressing cell attachment to achieve blood compatibility have been developed, including polyethylene glycol (PEG) and poly (2-methacryloyloxyethyl phosphorylcholine) (poly-MPC).[5,6] However, recent advances in medicine require the use of blood-compatible materials that exhibit non-blood cell attachment in an effort to isolate stem cells and circulating tumor cells (CTCs) from blood and to develop cardiovascular stent and artificial organs, such as endothelial cell-covered artificial blood vessels.[8,9]

To achieve materials with blood compatibility and the ability of non-blood cell attachment, cell-specific ligands are introduced with blood-compatible polymers during the development process.[8–10] Otherwise, heparin, which exhibits a strong anti-thrombosis effect, is induced in cell-attachable polymers.[9] Raynor et al.[10] modified PEG-covering titanium (Ti) with the Arg-Gly-Asp (RGD) peptide to improve Ti osseointegration. Wang et al.[8] prepared a Ti surface with blood compatibility and endothelial cell-attachment activity through the modification of heparin-VEGF-fibronectin (FN) for the development of cardiovascular stents. Knetsch et al.[9] prepared a heparin-incorporated copolymer of 1-vynylpyrrolidinone and *n*-butyl-methacrylate for vascular graft development. However, no blood-compatible polymers that exhibit non-blood cell-attachment activity through simple chemical structures have yet been developed.

We previously identified poly(2-methoxyethyl acrylate) (PMEA) and its analogous polymer, poly(tetrahydrofurfuryl acrylate) (PTHFA), as blood-compatible polymers.[7,11] PMEA and PTHFA substrates prevent platelet attachment through the suppression of fibrinogen adsorption and adsorption-induced deformation, which enables platelets to attach and activate.[7,12,13] We also reported that water structures, especially water molecules that are defined through differential scanning calorimetry as water that freezes at temperatures less than 0 °C in hydrated polymers (also called intermediate water), are important for the blood compatibility of PMEA and PTHFA. We show that the degrees of adsorption and deformation of fibrinogen are correlated with the amount of intermediate water in a copolymer of MEA and 2-hydroxyethyl methacrylate.[12] In addition, we show that the suppressions of fibrinogen adsorption and deformation are responsible for the blood compatibility of the PMEA substrate. However, it is unclear whether the adsorption and deformation of all proteins are suppressed on PMEA

Dr. T. Hoshiba, M. Nikaido, Prof. M. Tanaka
Graduate School of Science and Engineering
Yamagata University
4–3–16 Jonan, Yonezawa, Yamagata 992–8510, Japan
E-mail: tanaka@yz.yamagata-u.ac.jp
Dr. T. Hoshiba
International Center for Materials
Nanoarchitectonics (MANA)
National Institute for Materials Science
1–1 Namiki, Tsukuba, Ibaraki 305–0044, Japan

DOI: 10.1002/adhm.201300309

and other blood-compatible polymers substrates. It is possible that the degrees of suppression of protein adsorption and adsorption-induced deformation on blood-compatible polymers are altered for different types of proteins and blood-compatible polymers. We thus hypothesize whether all blood-compatible polymers actually prevent any type of cell attachment.

In this study, we examine whether cancer cells can attach to blood-compatible PMEA and PTHFA substrates and found that cancer cells are capable of attaching to PMEA and PTHFA blood-compatible substrates. Additionally, we investigate the attachment mechanisms of cancer cells to PMEA and PTHFA substrates, focusing primarily on integrin and adsorbed FN from serum. Moreover, we discusse the differences between cancer cells and platelets regarding the attachment mechanisms to PMEA and PTHFA substrates.

2. Results

2.1. Cancer Cell Attachment to PMEA and PTHFA Blood-Compatible Substrates

We first examined whether breast cancer cells (MDA-MB-231 and MCF-7) and mammary gland benign cells (MCF-10A) are capable of attaching to blood-compatible PMEA and PTHFA substrates. A cell attachment assay was performed using PMEA, PTHFA, polyethylene terephthalate (PET), MPC-*co*-butyl methacrylate copolymer (PMPC), and FN substrates in serum medium (**Figure 1**A, and Figures S1,S2, Supporting Information). MDA-MB-231, MCF-7, and MCF-10A cells initiated attachment to PET, PTHFA, PMEA, and FN after 20–60 min. In contrast, the majority of these cells did not attach to the PMPC substrate within 3 h. The differences in the attachment of MCF-10A cells between the PET, PTHFA, and PMEA substrates were lower than those found for MDA-MB-231 and MCF-7 cells. The attachment of MDA-MB-231 and MCF-7 cells to the PMEA substrate was 1.7- to threefold higher than that observed with the PET and PTHFA substrates. In contrast, the attachment of MCF-10A cells to the PMEA substrate was 1.1- to 1.4-fold greater than that observed with the PET and PTHFA substrates. However, the cell attachment of MDA-MB-231, MCF-7, and MCF-10A cells to the PMPC substrate was significantly (fivefold) lower than that observed with the PMEA, PTHFA, and PET substrates after 3 h of culture. Therefore, we concluded that these cells are capable of attaching to the PTHFA and PET substrates. The order of the attachment degrees of these MDA-MB-231, MCF-7, and MCF-10A cells after 3 h was found to be FN > PMEA > PTHFA, PET >> PMPC. The comparison of the MDA-MB-231, MCF-7, and MCF-10A cells revealed that the attachment of MCF-7 cells was lower than that observed with the MDA-MB-231 and MCF-10A cells. This difference appears to be due to the difference in the cell types. These results indicate that cancer cells can attach to blood-compatible PMEA and PTHFA substrates. To the best of our knowledge, these polymers are the first blood-compatible polymers to which cancer cells can attach.

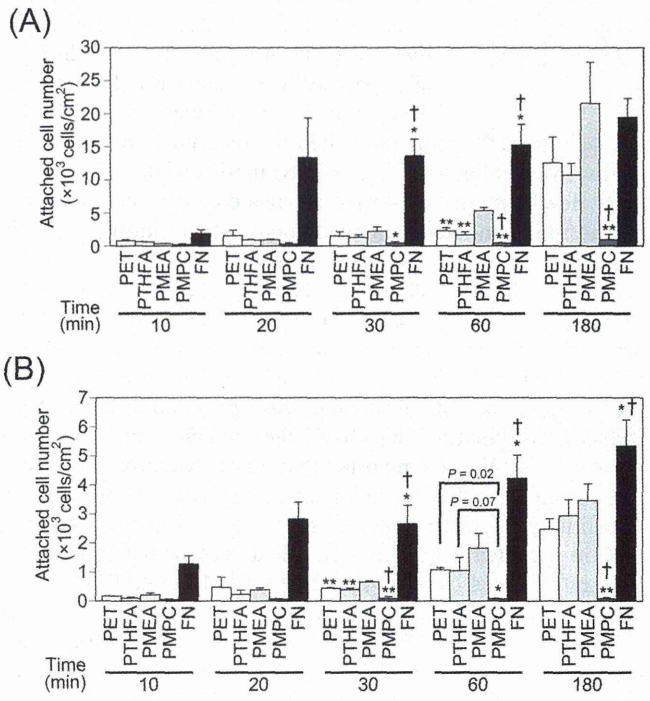

Figure 1. Cancer cell attachment to the blood-compatible polymers PMEA and PTHFA. A) MDA-MB-231 cell attachment. B) MCF-10A cell attachment. The data represent the means ± SD ($n = 3$). *: $P < 0.05$, **: $P < 0.01$ vs PMEA; †: $P < 0.05$ vs PTHFA and PET.

2.2. Cell Shapes on Polymer Substrates

It is hypothesized that the cell shape changes according to the manner through which it attaches. We thus compared the cell shape and the projected cell areas on the polymer substrates after 1 d of culture (**Figure 2**). On the FN substrate, the MDA-MB-231, MCF-7, and MCF-10A cells were well spread, and a large projected cell area was measured. Similar to the FN substrate, these three types of cells spread and exhibited large projected cell areas on the PTHFA and PET substrates. In contrast, on the PMEA substrate, the MDA-MB-231 and MCF-7 cells did not spread and showed significantly smaller projected cell areas compared with those obtained with the PTHFA, PET, and FN substrates (Figure 2A–C). Although the MCF-10A cells spread on the PMEA substrate, the projected cell area was significantly lower than that obtained with the PTHFA, PET, and FN substrates (Figure 2A,D). These results indicate that the spreading of the MDA-MB-231, MCF-7, and MCF-10A cells tended to be suppressed on PMEA. Additionally, it is possible that these cells use different cell-attachment mechanisms to attach to these different polymer substrates.

2.3. Cells Attach to the PMEA Substrate via Integrin-Dependent and -Independent Mechanisms

To investigate the attachment mechanisms of these cells to the blood-compatible PMEA and PTHFA substrates, we first examined whether these cells attached to these polymer substrates through integrin using a cell attachment assay with

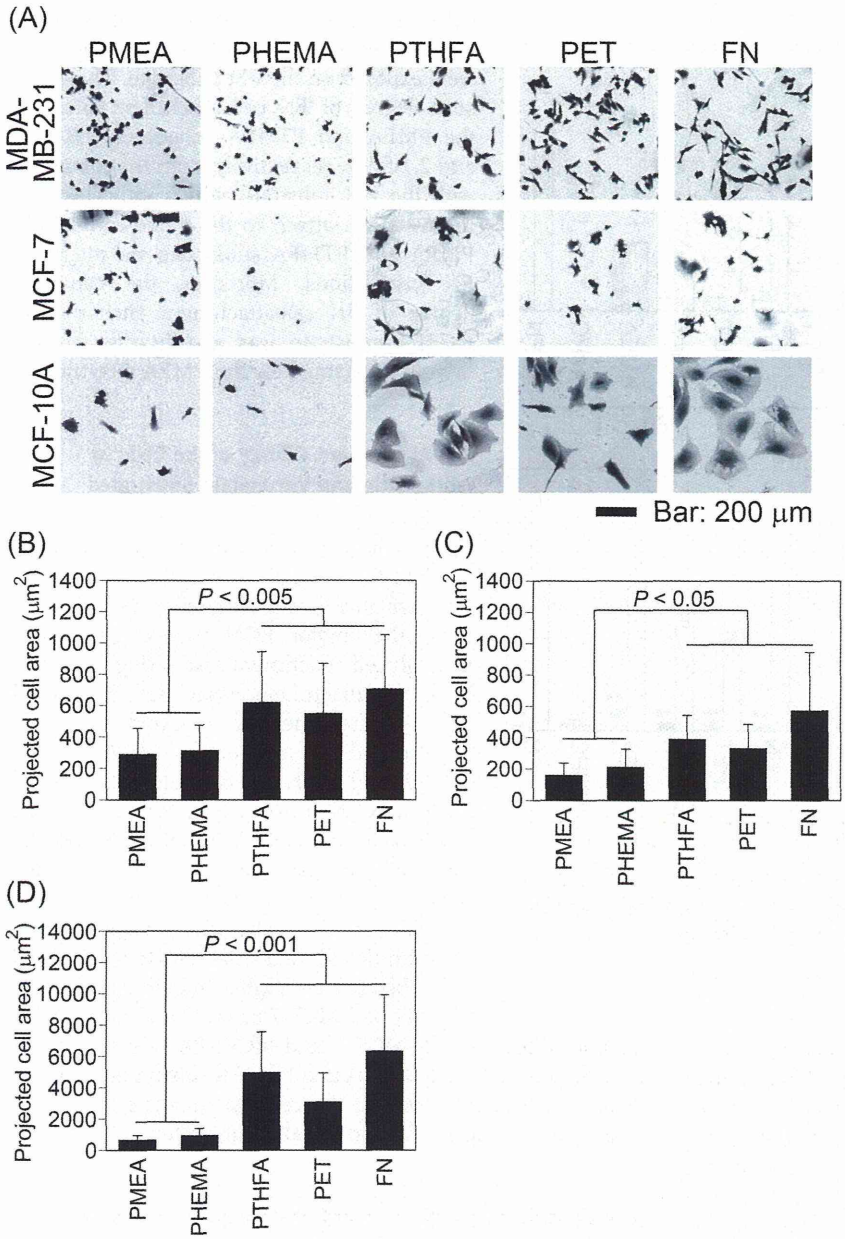

Figure 2. Cell morphology on blood-compatible substrates. A) Photographs of the cells stained with crystal violet. B–D) Projected cell area of B) MDA-MB-231, C) MCF-7, and D) MCF-10A cells. The data represent the means ± SD ($n = 54$).

ethylenediaminetetraacetic acid (EDTA), which is an inhibitor of integrin-dependent attachment (**Figure 3** and Figure S3, Supporting Information).[14] On the FN substrate, more than 95% of the attachment of MDA-MB-231, MCF-7, and MCF-10A cells was inhibited in the presence of EDTA, which suggests that all of the examined cells attach to the FN substrate via integrin. More than 85% of the attachment of MDA-MB-231, MCF-7, and MCF-10A cells to PET and PTHFA substrates was similarly inhibited in the presence of EDTA after 1 or 3 h (Figure 3 and Figure S3, Supporting Information). These results suggest that all of the examined cells mainly attach to the PET and PTHFA substrates via integrin.

Additionally, 87% of the MCF-10A cell attachment to the PMEA substrate was inhibited after 3 h in the presence of EDTA, which suggests that MCF-10A cells mainly attach to the PMEA substrate via integrin (Figure 3B). In contrast to the MCF-10A cell attachment to the PMEA substrate, the EDTA-induced inhibition percentages of the attachment of MDA-MB-231 and MCF-7 cells to PMEA substrates after 1 or 3 h were 35% and 55%, respectively (Figure 3A and Figure S3, Supporting Information). These results suggest that MDA-MB-231 and MCF-7 cells attach to the PMEA substrate via integrin-dependent and integrin-independent mechanisms.

To further confirm this attachment mechanism on polymer substrates, immunocytochemistry was used to analyze the vinculin localization as a marker of focal adhesions, which form at the sites of integrin-substrate interactions (**Figure 4** and Figure S4, Supporting Information).[15] The actin filaments were also observed. In MDA-MB-231 cells, evident focal adhesions were observed on PET, PTHFA, and FN substrates after 1 h. In contrast, few focal adhesions were observed in MDA-MB-231 cells attached to the PMEA substrate. Similarly to the MDA-MB-231 cells, evident focal adhesions were observed in MCF-7 cells attached to the PET, PTHFA, and FN substrates but not to the PMEA substrate after 24 h (Figure S4, Supporting Information). These results confirm the weaker integrin-dependent attachment of MDA-MB-231 and MCF-7 cells to the PMEA substrate compared with that obtained with the PET, PTHFA, and FN substrates.

In contrast to MDA-MB-231 and MCF-7 cells, evident focal adhesions were observed in MCF-10A cells attached to the PET, PTHFA, PMEA, and FN substrates after 24 h (Figure 4), which suggests that MCF-10A cells strongly attach via integrin even to the PMEA substrate. Few focal adhesions were observed on the PMEA substrates after 3 h, although the formation of focal adhesions was evident in MCF-10A cells attached to the PET, PTHFA, and FN substrates. These results suggest that the integrin-dependent attachment is delayed on the PMEA substrate, even for MCF-10A cells.

In addition to the integrin-dependent attachment, we examined attachment via syndecans, which are also major receptors for extracellular matrix (ECM) proteins on the cell surface.[16] To examine this possibility, the cell attachment assay was performed in the presence of EDTA and heparin (Figure S5, Supporting Information).[14] In the presence of only EDTA, the attachment of MDA-MB-231 and MCF-7 cells to the PMEA substrate was partially inhibited, whereas almost all of the attachment of these cells to the PTHFA, PET, and FN substrates was